

Electron-phonon interaction in GaAs/AlAs superlattices

Takuma Tsuchiya* and Tsuneya Ando

Institute for Solid State Physics, University of Tokyo, 7-22-1 Roppongi, Minato-ku, Tokyo 106, Japan

(Received 31 March 1992; revised manuscript received 21 July 1992)

Scattering rates of an electron in GaAs/AlAs superlattices are calculated in an envelope-function approximation which reproduces long-wavelength optical phonons almost completely. The polaron damping rate increases with decreasing layer-thickness at 300 K, while this dependence is smaller at 77 K. Intersubband relaxation rates decrease almost linearly as the layer thickness decreases. The results obtained in the dielectric continuum model agree quite well with those in the envelope-function approximation and even the bulk-phonon model explains the layer-thickness dependence reasonably well. This approximate model independence is explained by the completeness of the lattice vibration.

I. INTRODUCTION

High-mobility two-dimensional electron gas in modulation-doped structures has attracted much attention from the viewpoint of pure physics and device application. In devices with this structure, the most important scattering mechanism of electrons is due to the interaction with polar-optical phonons under usual operating conditions. Therefore, it is necessary and desirable to understand the electron-optical-phonon interaction in such heterostructures. Various models of optical phonons have been used to calculate the electron-optical-phonon scattering rates.¹⁻¹⁴ However, the results of these calculations are not consistent with each other and is confusing especially regarding the layer-thickness dependence of the scattering rates. In this paper, we calculate the rates in GaAs/AlAs superlattices in an envelope-function approximation,¹⁵ which reproduces long-wavelength optical phonons almost completely, and try to resolve such confusion. A brief account of this work was reported previously.¹⁶

At early stages, the electron-polar-optical-phonon interaction was calculated within a bulk-phonon model in which the usual Fröhlich interaction with bulk LO phonons of the material of the well layer is assumed.¹⁻⁹ In this model, the polaron damping rate, i.e., the scattering rate of an electron at the bottom of the ground subband, increases with a decrease of the thickness of the layers in which the electron is confined.

It is known that optical phonons are strongly modified by the presence of interfaces.¹⁷⁻²³ The simplest model that can demonstrate this fact is the so-called dielectric continuum model,²⁴⁻²⁷ in which each layer is replaced by a dielectric medium with a frequency-dependent dielectric constant. This model gives us two kinds of modes: confined modes and interface modes. The confined modes have amplitudes only in one kind of layer and frequencies of either bulk LO or TO phonons. On the other hand, the interface modes, sometimes called Fuchs-Kliwer modes,²⁸ have frequencies strongly dependent on the wave vector and have amplitudes in both kinds of layers decaying exponentially away from the interfaces. Various aspects of electron-phonon interactions have

been investigated in this model.^{10-14,29,30} For example, Mori and Ando¹² calculated the polaron damping rate and magnetophonon-resonance spectra for GaAs/AlAs single heterostructures and quantum wells at 300 K. They found that the contribution of the confined modes decreases and that of the interface modes increases with decreasing layer thickness. The total scattering rate turned out to be very similar to that of the bulk-phonon model. They showed that this is closely related to a sum rule existing among the form factors for the electron-phonon matrix element.

Phonons in superlattices have been observed directly in Raman-scattering experiments and the results of these experiments have been analyzed on the basis of a linear-chain model. In spite of the simplicity, this model is usually sufficient in describing modes with a wave vector perpendicular to layers. It was applied to GaAs/AlAs superlattices and showed that optical phonons are completely confined within either GaAs or AlAs layers.³¹⁻⁴¹ This result is consistent with that of the dielectric continuum model, since all optical modes are confined even in the dielectric continuum model when the wave vector is perpendicular to layers. However, if we look at the results more carefully, there is a significant contrast. In the dielectric continuum model, the displacement of ions in the z direction perpendicular to the layers can be maximum at the interfaces. In the linear-chain model, however, the displacement vanishes at the interfaces.

This disagreement has led to a strong doubt regarding the validity of the dielectric continuum model and to proposals of various phonon models. Sawaki⁴² calculated the scattering rates in GaAs/AlAs superlattices, assuming that confined electrons interact only with LO phonons confined to the same layer and having vanishing displacements at the interfaces. The results showed that the polaron damping rate decreases with a narrowing of the well layer in contrast to the result in the dielectric continuum model. Ridley⁴³ imposed an artificial boundary condition on the confined modes of the dielectric continuum model that the z component of the displacement and the z derivative of the parallel components should vanish at the interfaces on the basis of the result in a hydrodynamic boundary-condition model.⁴⁴ The resulting polaron

damping rate decreases almost linearly with decreasing layer thickness and its absolute value is much smaller than that obtained in the dielectric continuum model. Huang and Zhu⁴⁵ proposed another boundary condition that both value and z derivative of the potential associated with lattice displacement should vanish at interfaces. This leads to vanishing displacement at the interfaces in agreement with the linear-chain model. This model was also used for the calculation of the scattering rate and gave a different answer.⁴⁶

The purpose of this paper is to resolve such controversies and clarify the nature of the electron-optical-phonon interaction in semiconductor superlattices. We calculate the electron-phonon scattering rate in GaAs/AlAs superlattices using the envelope-function approximation which reproduces the results obtained by lattice-dynamical calculations quite well,¹⁵ and compare the results with those obtained in different models. Although microscopic calculation of the scattering rates is possible,⁴⁷ a reliable continuum model of optical phonons in superlattices is highly desirable because it can serve as a Fröhlich model in the bulk.

This paper is organized as follows. In Sec II the envelope-function approximation is introduced. The electron-phonon interaction in GaAs/AlAs superlattices is calculated in Sec. III. The method of calculation is presented in Sec. III A and numerical results are shown in Sec. III B together with those in the bulk-phonon model and the dielectric continuum model. In Sec. III C the completeness of phonon modes is shown to be the origin of the fact that scattering rates are nearly independent of different models. Section IV is devoted to a summary.

II. ENVELOPE-FUNCTION APPROXIMATION

In the envelope-function approximation, we consider $\mathbf{U}(\mathbf{r}) = \mathbf{U}_c(\mathbf{r}) - \mathbf{U}_a(\mathbf{r})$, where $\mathbf{U}_c(\mathbf{r})$ and $\mathbf{U}_a(\mathbf{r})$ is an en-

$$H(q_x, q_y, q_z) = \begin{pmatrix} Aq_x^2 + B(q_y^2 + q_z^2) & Cq_x q_y & Cq_x q_z \\ Cq_y q_x & Aq_y^2 + B(q_z^2 + q_x^2) & Cq_y q_z \\ Cq_z q_x & Cq_z q_y & Aq_z^2 + B(q_x^2 + q_y^2) \end{pmatrix}, \quad (2.6)$$

where $\mathbf{q} = (q_x, q_y, q_z)$ is a wave vector. The parameters A , B , and C can be determined so as to reproduce the bulk dispersion in a long-wavelength limit. We determine these parameters as $A \approx -2.14 \times 10^{-2}$, $B \approx -0.75 \times 10^{-2}$, and $C \approx -1.38 \times 10^{-2}$ for GaAs and $A \approx -1.85 \times 10^{-2}$, $B \approx -0.67 \times 10^{-2}$, and $C \approx -1.18 \times 10^{-2}$ for AlAs in units of $\omega_{\text{TO}}^2 a^2$.

For these parameters, phonons in the bulk have an isotropic dispersion relation, and longitudinal and transverse modes are completely decoupled even for wave vectors in nonsymmetry directions. As discussed in Ref. 15, a valence force-field model gives phonon dispersions which are slightly anisotropic in GaAs and AlAs. However, the anisotropy is not so appreciable and errors arising from the approximation are expected to be small.

For GaAs/AlAs superlattices, we can safely neglect

velope of the displacement of cations and anions, respectively. In each layer, the envelope satisfies the equation

$$(\omega^2 - \omega_{\text{TO}}^2) \mathbf{U}(\mathbf{r}) = H \left[\frac{\partial}{i\partial x}, \frac{\partial}{i\partial y}, \frac{\partial}{i\partial z} \right] \mathbf{U}(\mathbf{r}) - \frac{Ze}{M_r} \mathbf{E}(\mathbf{r}), \quad (2.1)$$

where ω is frequency, ω_{TO} is the frequency of the TO phonon of the bulk material of this layer, and M_r is the reduced mass defined as $M_r = M_c M_a / (M_c + M_a)$ with M_c and M_a the mass of a cation and an anion, respectively. The effective charge of an ion Ze is given by

$$Ze = \left[\frac{M_r}{n} \right]^{1/2} \epsilon_\infty \omega_{\text{LO}} \left[\frac{1}{4\pi} \left[\frac{1}{\epsilon_\infty} - \frac{1}{\epsilon_0} \right] \right]^{1/2}, \quad (2.2)$$

with ω_{LO} the frequency of the LO phonon of the bulk, ϵ_∞ the high-frequency dielectric constant which is assumed to be independent of the constituent materials, ϵ_0 ($= \epsilon_\infty \omega_{\text{LO}}^2 / \omega_{\text{TO}}^2$) the static dielectric constant, and n the number of cation-anion pairs in a unit volume, i.e., $n = 4/a^3$ for zinc-blende crystals where a is the lattice constant.

The macroscopic electric field $\mathbf{E}(\mathbf{r})$ is determined through

$$\mathbf{E}(\mathbf{r}) = -\nabla \phi(\mathbf{r}) \quad (2.3)$$

with the electrostatic potential

$$\phi(\mathbf{r}) = \int d\mathbf{r}' \frac{\mathbf{P}(\mathbf{r}') \cdot (\mathbf{r} - \mathbf{r}')}{\epsilon_\infty |\mathbf{r} - \mathbf{r}'|^3}, \quad (2.4)$$

where $\mathbf{P}(\mathbf{r})$ is the polarization given by

$$\mathbf{P}(\mathbf{r}) = nZe \mathbf{U}(\mathbf{r}). \quad (2.5)$$

Further, H is a 3×3 matrix Hamiltonian given by

the lattice mismatch and set $a = 5.653 \text{ \AA}$ for both GaAs and AlAs. For simplicity, we use $\epsilon_\infty = 9.53$, which is the average of ϵ_∞ of GaAs and AlAs. When ϵ_∞ varies between layers, the relation between the polarization and the electrostatic potential becomes far more complicated because of necessary image charge effects. Other parameters are summarized in Table I.

Because frequencies of bulk optical modes of GaAs and AlAs do not overlap in energy, we can clearly separate optical phonons into two kinds: GaAs-like modes and AlAs-like modes. The GaAs-like modes have a frequency close to that of optical phonons of bulk GaAs and their amplitude of displacement is almost entirely confined to GaAs layers. Furthermore, the amount of dispersion, i.e., the bandwidth, of bulk phonons is smaller than the energy separation between optical phonons in bulk GaAs

TABLE I. Parameters used for the present calculations. The mass of anions and cations are denoted by M_a and M_c , respectively, M_r is the reduced mass of anion-cation pairs, $\hbar\omega_{LO}$ and $\hbar\omega_{TO}$ are the energies of the bulk LO and TO phonons, respectively.

	M_c (a.u.)	M_a (a.u.)	M_r (a.u.)	$\hbar\omega_{LO}$ (meV)	$\hbar\omega_{TO}$ (meV)
GaAs	69.72	74.92	36.11	36.19	33.30
AlAs	26.98	74.92	19.84	50.10	44.75

and AlAs. Therefore, we can neglect the presence of dispersion of phonons in the AlAs layer, i.e., set $A=B=C=0$ in Eq. (2.6) for the GaAs-like phonons. This means that we employ the dielectric continuum model in the AlAs layer. The same applies to the AlAs-like modes. We impose boundary conditions for the envelope in the GaAs layer that should vanish at a boundary plane near the interfaces. In this paper, we assume that the boundary plane is at the interfacial As plane, although the actual boundary plane is known to be shifted by roughly a monolayer thickness or less. This shift is not important except in superlattices with extremely small layer thickness.

The validity of the boundary conditions mentioned above has been justified microscopically.⁴⁸ These boundary conditions become inappropriate and more sophisticated conditions should be introduced when frequencies of optical phonons of constituent materials overlap each other.⁴⁸ The envelope-function approximation reduces to the dielectric continuum model when we set the parameters of the bulk dispersion as $A=B=C=0$ in both layers. Furthermore, neglecting the differences of parameters, ω_{TO} , Z_e , etc., between layers, we can get the results in the bulk-phonon model.

We choose the origin of z in such a way that a GaAs layer occupies the region $0 < z < d_1$ and an AlAs layer $-d_2 < z < 0$ and let d represent the superlattice period given by $d = d_1 + d_2$. We introduce a reduced envelope $\mathbf{W}(\mathbf{r})$, which is convenient for calculating phonon modes in inhomogeneous materials, defined by

$$\mathbf{W}(\mathbf{r}) = \sqrt{nM_r}(\mathbf{r})\mathbf{U}(\mathbf{r}). \quad (2.7)$$

Because of the periodicity, it can be written as

$$\mathbf{W}_{j\mathbf{q}}(\mathbf{r}) = \sum_{m=0}^{N-1} \mathbf{w}_{j\mathbf{q}}(z-md) \frac{\exp(iq_z md)}{\sqrt{N}} \frac{\exp(i\mathbf{q}_{\parallel} \cdot \mathbf{r}_{\parallel})}{L}, \quad (2.8)$$

where $\mathbf{w}_{j\mathbf{q}}(z)$ is defined only in the region $-d_2 < z < d_1$, L is the linear dimension of the system, $N (=L/d)$ is the total number of superlattice periods, $\mathbf{r} = (\mathbf{r}_{\parallel}, z) = (x, y, z)$, the mode is specified by the index j , and the wave vector $\mathbf{q} = (\mathbf{q}_{\parallel}, q_z) = (q_x, q_y, q_z)$ ($-\pi/d < q_z < \pi/d$).

Let us consider modes with dominant amplitude in the GaAs layer. Within the GaAs layer, the reduced displacement is expanded into

$$w_{j\mathbf{q}}^{\alpha}(z) = \sum_{p=1}^{N_a} C_p^{\alpha} \left[\frac{2}{d_1} \right]^{1/2} \sin \left[\frac{p\pi}{d_1} z \right], \quad (2.9)$$

where C_p^{α} is the expansion coefficient and $\alpha (=x, y, z)$

represents the direction of displacement. We have introduced a cutoff, N_a , equal to the number of layers of anion-cation pairs in this layer, in order to make the number of the optical modes in this approximation equal to that in the actual superlattices. This cutoff is important only when the layer thickness is small.

Because we employ the dielectric continuum model in the AlAs layer, the displacement in the AlAs layer is proportional to the macroscopic electric field, which decays exponentially [$\propto \exp(\pm q_{\parallel} z)$] away from the interface. Therefore, we have

$$w_{j\mathbf{q}}^{\alpha}(z) = \left[C_S^{\alpha} \left[\frac{2q_{\parallel}}{\sinh(q_{\parallel}d_2) + q_{\parallel}d_2} \right]^{1/2} \times \cosh[q_{\parallel}(z + d_2/2)] + C_A^{\alpha} \left[\frac{2q_{\parallel}}{\sinh(q_{\parallel}d_2) - q_{\parallel}d_2} \right]^{1/2} \times \sinh[q_{\parallel}(z + d_2/2)] \right], \quad (2.10)$$

for $-d_2 < z < 0$, where the subscripts S and A denote symmetric and antisymmetric components, respectively.

Using Eqs. (2.1)–(2.10), we obtain an eigenvalue problem for $3(N_a + 2)$ unknown coefficients C 's and phonon frequencies. Because the dispersion is isotropic within the plane parallel to the interface, we can choose \mathbf{q} in the xz plane. The y component of displacement is decoupled from the x and z component, induces no macroscopic electric field, and therefore can be ignored completely. Thus, the eigenvalue problem can be reduced to the $2(N_a + 2)$ dimension. The same procedure is applicable to obtaining AlAs-like phonons.

We normalize the reduced displacement in one period as

$$\int_{-d_2}^{d_1} |\mathbf{w}_{j\mathbf{q}}(z)|^2 dz = 1. \quad (2.11)$$

Then, the reduced displacement can be written in a form of second quantization as

$$\mathbf{W}(\mathbf{r}) = \sum_{j,\mathbf{q}} \left[\frac{\hbar}{2\omega_j(\mathbf{q})} \right]^{1/2} [\mathbf{W}_{j\mathbf{q}}(\mathbf{r})b_{j\mathbf{q}} + \mathbf{W}_{j\mathbf{q}}^*(\mathbf{r})b_{j\mathbf{q}}^{\dagger}], \quad (2.12)$$

where $b_{j\mathbf{q}}$ and $b_{j\mathbf{q}}^{\dagger}$ are the destruction and creation opera-

tors for a phonon of mode j and wave vector \mathbf{q} and $\omega_j(\mathbf{q})$ is its frequency. This envelope-function approximation reproduces long-wavelength optical phonons almost exactly as demonstrated already in Ref. 15.

$$\sum_j W_{j\mathbf{q}}^\alpha(\mathbf{r}) W_{j\mathbf{q}}^{\alpha'*}(\mathbf{r}') = \delta_{\alpha\alpha'} \sum_{m=0}^{N-1} \sum_{m'=0}^{N-1} \delta[z-md - (z'-md)] \frac{\exp[iq_z(m-m')d]}{N} \frac{\exp[i\mathbf{q}_\parallel \cdot (\mathbf{r}_\parallel - \mathbf{r}'_\parallel)]}{L^2} \quad (2.13)$$

corresponding to the completeness of the phonon modes, where the summation over j runs over both GaAs- and AlAs-like modes.

When energy of light is close to or smaller than that of optical phonons, interaction between the light and the phonons becomes important and they are coupled into a set of modes called polariton.⁴⁹ This polariton effect can be important also in semiconductor superlattices.⁵⁰ For GaAs, for example, it is appreciable when the wavelength of light and optical phonons is larger than $3 \times 10^5 \text{ \AA}$. For damping rates, however, the important wavelength is determined by the energy and momentum conservation for interaction with electrons and is much smaller. For example, the typical wavelength determining the polaron damping rate is about $2.5 \times 10^2 \text{ \AA}$ which is three orders of magnitude smaller than that of polaritons. Thus, the polariton effect can be neglected completely in the present problem.

III. ELECTRON-PHONON INTERACTION

A. Scattering rates

The scattering rate of an electron in subband η ($=1, 2, \dots$) at wave vector \mathbf{k} to subband η' by phonon emission and absorption is represented by Fermi's golden rule as

$$\frac{1}{\tau_{\eta'\eta\pm}(\mathbf{k})} = \frac{2\pi}{\hbar} \sum_j \sum_{\mathbf{q}} |M_{\eta'\eta j\mathbf{q}\pm}(\mathbf{k})|^2 \{n[\omega_j(\mathbf{q})] + \frac{1}{2} \pm \frac{1}{2}\} \times \delta[E_f - E_i \pm \hbar\omega_j(\mathbf{q})], \quad (3.1)$$

with

$$n(\omega) = \left[\exp\left(\frac{\hbar\omega}{k_B T}\right) - 1 \right]^{-1}, \quad (3.2)$$

where E_i and E_f are the electron energy of initial and final states, respectively, k_B is the Boltzmann constant, and T is the temperature. The upper and lower signs represent the contributions of phonon emission and absorption processes, respectively. The matrix element M of electron-phonon interaction can be expressed as

$$M_{\eta'\eta j\mathbf{q}\pm}(\mathbf{k}) = \int d\mathbf{r} \psi_{\eta'\mathbf{k}\mp\mathbf{q}}^*(\mathbf{r}) (-e) \phi_{j\mathbf{q}}(\mathbf{r}) \psi_{\eta\mathbf{k}}(\mathbf{r}), \quad (3.3)$$

where $\phi_{j\mathbf{q}}(\mathbf{r})$ is the electrostatic potential associated with a phonon with mode j and wave vector \mathbf{q} .

We assume that an electron is completely confined to the GaAs layer and adopt the wave function

$$\psi_{\eta\mathbf{k}}(\mathbf{r}) = \sum_{m=0}^{N-1} \psi_\eta(z-md) \frac{\exp(ik_z md)}{\sqrt{N}} \frac{\exp(i\mathbf{k}_\parallel \cdot \mathbf{r}_\parallel)}{L}, \quad (3.4)$$

It should be noticed that as long as the present envelope-function approximation is valid, the solution of the eigenvalue problem $\mathbf{W}_{j\mathbf{q}}(\mathbf{r})$ satisfies within a good accuracy the closure relation

with

$$\psi_\eta(z) = \left[\frac{2}{d_1} \right]^{1/2} \sin\left[\frac{\eta\pi}{d_1} z \right] \quad (3.5)$$

for $0 < z < d_1$ and $\psi_\eta(z) = 0$ for $-d_2 < z < 0$, where $\mathbf{k} = (\mathbf{k}_\parallel, k_z) = (k_x, k_y, k_z)$ ($-\pi/d < k_z < \pi/d$). The corresponding energy is independent of k_z and is given by

$$E_\eta(\mathbf{k}_\parallel) = \frac{\hbar^2}{2m^*} \left[\frac{\eta\pi}{d_1} \right]^2 + \frac{\hbar^2 k_\parallel^2}{2m^*}, \quad (3.6)$$

where m^* is the effective mass at the conduction-band bottom. This assumption is valid when the thickness of the barrier and well layers is sufficiently large. For GaAs/AlAs systems, the critical thickness is quite small (estimated as $\sim 25 \text{ \AA}$ using the effective-mass approximation) because of the large discontinuity of the conduction-band bottom ($\sim 1 \text{ eV}$). The explicit expression for the matrix element is given in the Appendix.

We will calculate the scattering rate of an electron at the bottom of the ground subband, i.e., the polaron damping rate. Only the absorption process contributes to the damping rate. Furthermore, if the splitting between the ground and first excited subbands is larger than the phonon energy, there are no intersubband processes. Therefore it can be calculated from Eq. (3.1) with $M_{11j\mathbf{q}-}(0)$ and $E_f - E_i = E_1(q_\parallel) - E_1(0) = \hbar^2 q_\parallel^2 / 2m^*$. For scattering of an electron at the bottom of the first excited subband, the following three processes are possible, if the subband splitting is larger than the phonon energy: (i) intrasubband transition with phonon absorption, (ii) intersubband transition to the ground subband with phonon absorption, (iii) intersubband transition to the ground subband with phonon emission. These rates can be calculated by Eq. (3.1) with $M_{12j\mathbf{q}\pm}(0)$ and $E_f - E_i = E_1(q_\parallel) - E_2(0)$ and with $M_{22j\mathbf{q}-}(0)$ and $E_f - E_i = E_2(q_\parallel) - E_2(0) = \hbar^2 q_\parallel^2 / 2m^*$ for the intersubband and the intrasubband transition, respectively. The damping rate Γ is related to the corresponding relaxation time τ defined in Eq. (3.1) through $\Gamma = \hbar/2\tau$.

B. Numerical results

1. Polaron damping

Figure 1 compares the layer-thickness dependence of the polaron damping rate in the GaAs/AlAs superlattices for $d_1 = d_2$ at 300 K calculated in the envelope-function approximation, the dielectric continuum model, and the bulk-phonon model. The figure contains the separate contributions of GaAs-like and AlAs-like modes

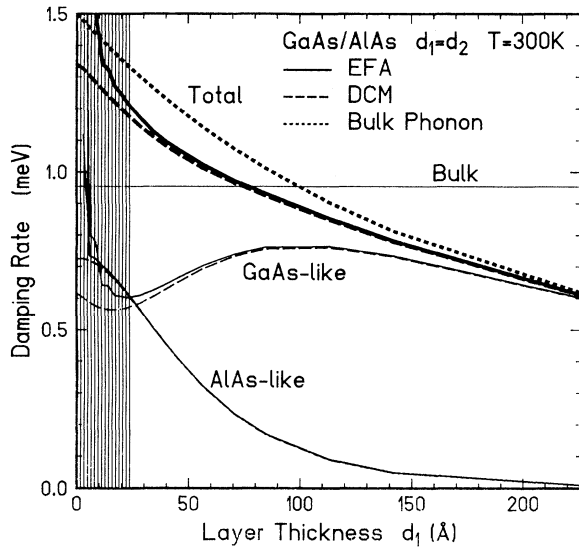


FIG. 1. Layer-thickness d_1 dependence of the polaron damping rate calculated in the envelope-function approximation (solid line), the dielectric continuum model (dashed line), and the bulk-phonon model (dotted line) at 300 K. The thickness of barrier layer d_2 is equal to that of the well layer d_1 . For the envelope-function approximation and the dielectric continuum model, the separate contributions of GaAs-like and AlAs-like modes are also shown. The thin horizontal line represents the damping rate in bulk GaAs. In the hatched region, the assumption that an electron is completely confined to the well layer becomes inappropriate.

for the envelope-function approximation and the dielectric continuum model. In the envelope-function approximation, we can calculate the rates only at an integral multiple of one monolayer thickness $a/2$ and straight lines are drawn between these points. The results calculated in these three models are very similar. In particular, the result in the dielectric continuum model is almost in agreement with that in the envelope-function approximation. The damping rate increases with the decrease of the layer thickness. This is because the electron confinement tends to enhance the electron-phonon interaction.

In the thin-layer region ($d_1 < 15 \text{ \AA}$), the result in the envelope-function approximation shows a zigzag dependence on layer thickness and exhibits a sudden increase for very small d_1 . This increase is due to a lowering of phonon energies by the confinement effect and resulting increase in the number of thermally activated phonons. This effect is overestimated because of the approximation of parabolic phonon dispersion and the assumption that the effective layer thickness is not $(N_a + 1)a/2$ or $(N_1 + 0.5)a/2$ as in Ref. 15 but $N_a a/2$. The zigzag shape is caused by the reduction in the number of phonon modes with decreasing layer thickness. (Three optical modes disappear, whenever the layer thickness decreases by one monolayer.) Strictly speaking, in the hatched region $d_1 < 25 \text{ \AA}$, electrons are no longer confined in GaAs layers and the actual damping rate is expected to be

smaller than the above results. Both the zigzag dependence and the sudden increase are expected to remain to some extent, because they are due to changes in phonon properties.

In systems with a thick layer ($d_1 > 150 \text{ \AA}$), the contribution of AlAs-like modes is much smaller than that of GaAs-like modes, but it increases as the layer thickness decreases and may even exceed the contribution of GaAs-like modes. In Fig. 1, we also show the damping rate in *bulk* GaAs, $\hbar\omega_{LO}\alpha_F n(\omega_{LO})$, i.e., in the case that there is no confinement for both electrons and phonons, where

$$\alpha_F = \frac{1}{2} \left[\frac{1}{\epsilon_\infty} - \frac{1}{\epsilon_0} \right] \frac{e^2}{\hbar\omega_{LO}} \left[\frac{2m^*\omega_{LO}}{\hbar} \right]^{1/2} \quad (3.7)$$

is the Fröhlich coupling constant.

In the region $d_1 > 80 \text{ \AA}$, the damping in the superlattice is smaller than in the bulk. This difference increases with the layer thickness. However, when $d_1 > 170 \text{ \AA}$, the subband splitting between the lowest and first excited subbands is smaller than the phonon energy and intersubband transitions should strongly increase the damping rate beyond the bulk value. Hence, the reduction of Γ in the superlattice from Γ in the bulk is at most about 20%.

At 77 K, Γ is much smaller than at 300 K as shown in Fig. 2 because of the decrease of the number $n(\omega)$ of thermally activated phonons [$n(\omega_{LO}) = 0.33$ and 0.17 for GaAs and AlAs, respectively, at 300 K and $n(\omega_{LO}) = 4.3 \times 10^{-3}$ and 5.3×10^{-4} at 77 K]. The difference between Γ calculated in the envelope-function approximation and in the bulk-phonon model is larger than at 300 K. This arises from the fact that the reduction of the number of higher-energy AlAs-like phonons compared to that of GaAs-like phonons is not properly taken into account in the bulk phonon model. The difference of Γ between the envelope-function approxima-

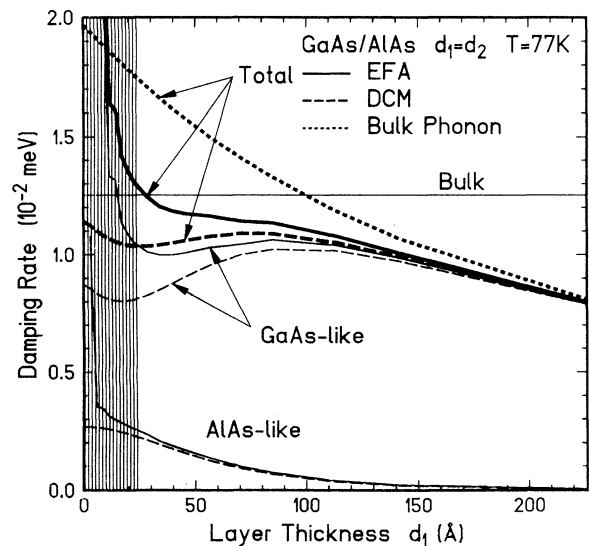


FIG. 2. Calculated layer-thickness d_1 dependence of the polaron damping rate at 77 K. $d_2 = d_1$.

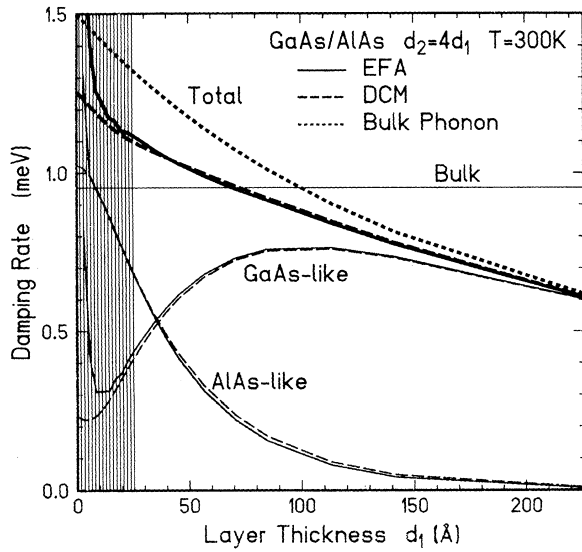


FIG. 3. Calculated layer-thickness d_1 dependence of the polaron damping rate at 300 K. $d_2=4d_1$.

tion and the dielectric continuum model is also slightly larger than at 300 K. In the dielectric continuum model Γ is underestimated, because the reduction of the phonon energy due to confinement is not considered at all. The region in which Γ in superlattices is smaller than in bulk GaAs extends up to $d_1 > 30$ Å.

In Figs. 3 and 4, we show the results in the case $d_2=4d_1$. At 300 K, the contribution of the GaAs-like modes is smaller than that in the case $d_2=d_1$ and the contribution of the AlAs-like modes is larger. Consequently, the total damping rate does not change much. At 77 K, the reduction of the damping rate from that in bulk GaAs is slightly more pronounced than for $d_2=d_1$.

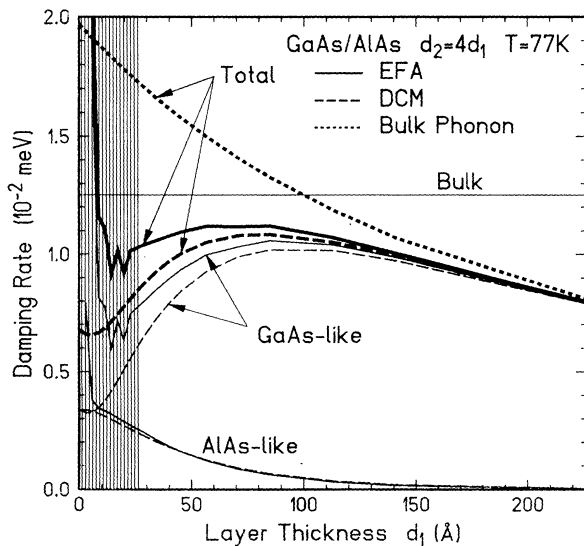


FIG. 4. Calculated layer-thickness d_1 dependence of polaron damping rate at 77 K. $d_2=4d_1$.

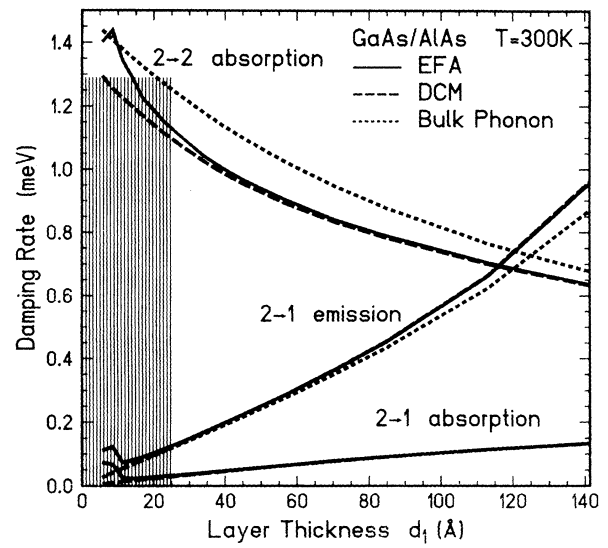


FIG. 5. Layer-thickness d_1 dependence of damping rate of an electron at the bottom of the first excited subband calculated in the envelope-function approximation (solid lines), the dielectric continuum model (dashed lines), and the bulk-phonon model (dotted lines) at 300 K. $d_2=d_1$.

2. Intersubband relaxation

Figure 5 shows calculated damping rates of an electron at the bottom of the first excited subband at 300 K as a function of the layer thickness. The damping rate of intrasubband transitions is similar to the polaron damping rate given in Fig. 1. The damping rate for the intersubband transition with phonon absorption is a sublinear

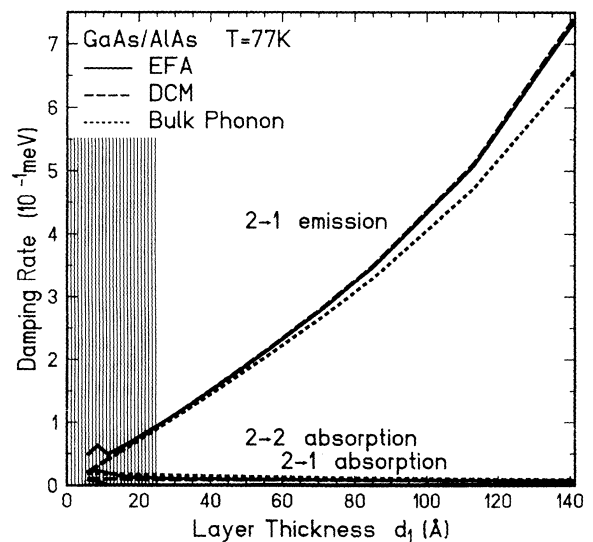


FIG. 6. Layer-thickness d_1 dependence of damping rate of an electron at the bottom of the first excited subband at 77 K. The contribution of intersubband transition due to phonon emission is much larger than those of the other two processes.

function of d_1 and that with phonon emission is a super-linear function of d_1 . This difference comes from that of the wave numbers where the energy conservation is satisfied. The results in different approximations are almost indistinguishable for the intersubband absorption process, while in the emission process the result in the bulk-phonon model is slightly lower. This is again due to differences in the phonon frequencies.

Figure 6 shows calculated damping rates at 77 K. The damping rate due to phonon absorption processes is smaller by roughly two orders of magnitude than at 300 K, while that of emission processes remains almost the same.

C. Discussion

In the preceding section, it has been found that the results in the dielectric continuum model agree quite well with those in the envelope-function approximation and even the bulk-phonon model explains the layer thickness dependence reasonably well. In order to clarify the reason, we separate the total scattering rate into contributions of different phonon modes. One way to achieve this separation is to consider the Eliashberg function $\alpha^2(\omega)F(\omega)$ describing the contribution of phonons having frequency ω , defined by

$$\Gamma = \int d\omega \alpha^2(\omega)F(\omega)n(\omega), \quad (3.8)$$

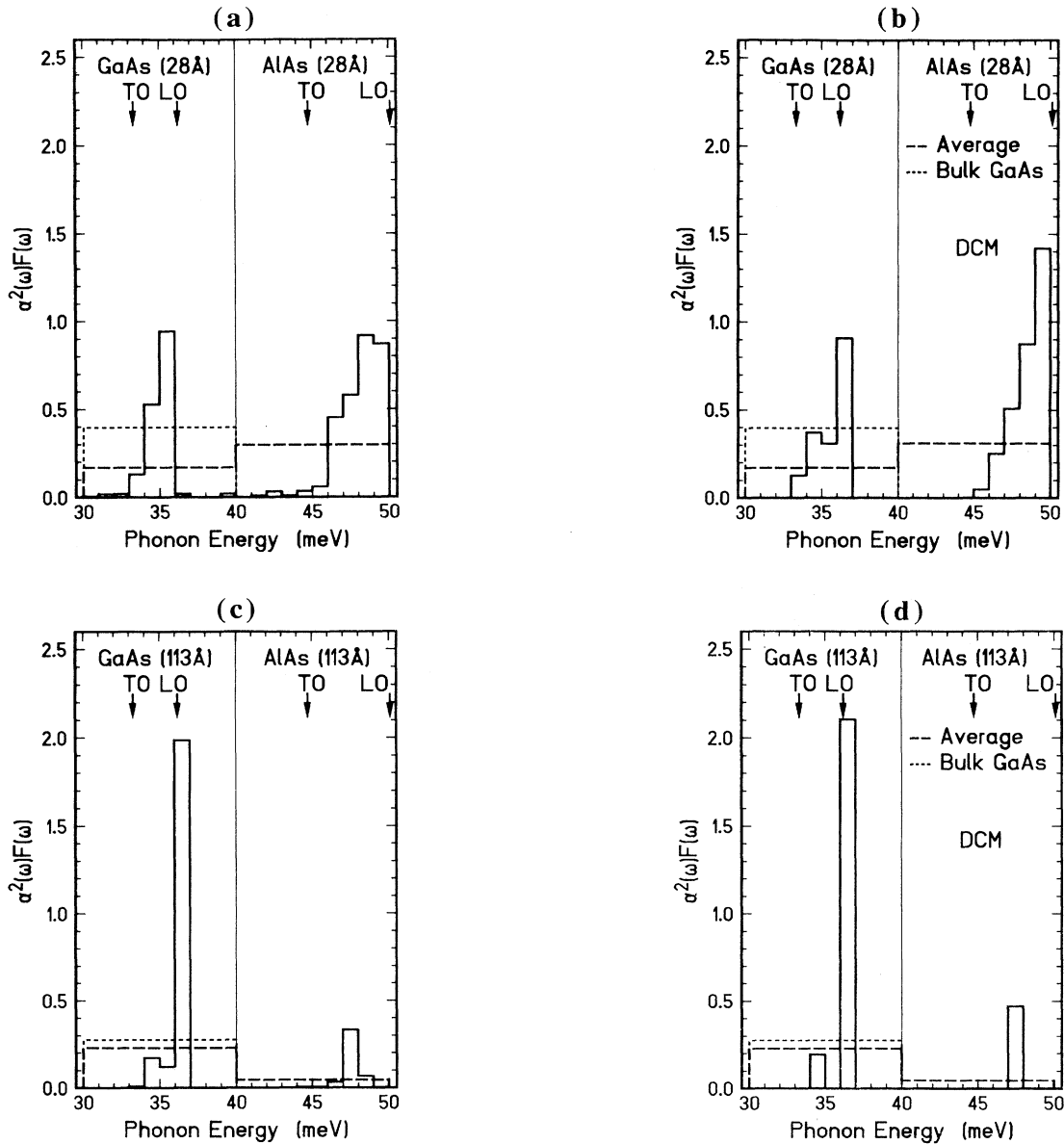


FIG. 7. Histogram of the Eliashberg function for the polaron damping rate in a $(\text{GaAs})_{10}(\text{AlAs})_{10}$ superlattice calculated in the envelope-function approximation (a) and the dielectric continuum model (b), and in a $(\text{GaAs})_{40}(\text{AlAs})_{40}$ superlattice in the envelope-function approximation (c) and the dielectric continuum model (d). Solid lines show results when the frequency interval is 1 meV and dashed lines 10 meV. The dotted lines represent the result in the bulk-phonon model.

where $\alpha^2(\omega)$ is an effective electron-phonon coupling function and $F(\omega)$ is the phonon density of states. For the polaron damping rate, we have from Eq. (3.1)

$$\alpha^2(\omega)F(\omega) = \pi \sum_j \sum_q |M_{11jq-}(0)|^2 \times \delta[\omega_j(\mathbf{q}) - \omega] \delta \left[\frac{\hbar^2 q_{\parallel}^2}{2m^*} - \hbar\omega \right]. \quad (3.9)$$

Figure 7 gives histograms of $\alpha^2(\omega)F(\omega)$ given by

$$E_n = \frac{1}{\Delta\omega} \int_{\omega_n}^{\omega_n + \Delta\omega} d\omega \alpha^2(\omega)F(\omega) \quad (3.10)$$

with $\omega_n = n\Delta\omega$ (n is an integer) for GaAs/AlAs superlattices with $d_1 = d_2 = 28$ Å and $d_1 = d_2 = 113$ Å. In these figures, we show the results with $\Delta\omega = 1$ meV and $\Delta\omega = 10$ meV. For $\Delta\omega = 10$ meV the total scattering rate is separated into the contribution of GaAs-like modes

$$\frac{1}{\tau_{\eta'\eta_{\pm}}(\mathbf{k})} = \frac{2\pi e^2}{\hbar} \sum_j \sum_q \delta[E_i - E_f \pm \hbar\omega_j(\mathbf{q})] \{n[\omega_j(\mathbf{q})] + \frac{1}{2} \pm \frac{1}{2}\} \times \int dr_1^3 \int dr_1'^3 \int dr_2^3 \int dr_2'^3 \psi_{\eta'\mathbf{k}+\mathbf{q}}^*(\mathbf{r}_1) \psi_{\eta\mathbf{k}}(\mathbf{r}_1) \psi_{\eta'\mathbf{k}+\mathbf{q}}(\mathbf{r}_2) \psi_{\eta\mathbf{k}}^*(\mathbf{r}_2) \times \frac{(\mathbf{r}_1 - \mathbf{r}_1') \cdot \mathbf{P}_{jq}(\mathbf{r}_1')}{\epsilon_{\infty} |\mathbf{r}_1 - \mathbf{r}_1'|^3} \frac{(\mathbf{r}_2 - \mathbf{r}_2') \cdot \mathbf{P}_{jq}^*(\mathbf{r}_2')}{\epsilon_{\infty} |\mathbf{r}_2 - \mathbf{r}_2'|^3}, \quad (3.11)$$

with

$$\mathbf{P}_{jq}(\mathbf{r}) = \mathbf{W}_{jq}(\mathbf{r}) \sum_{l=1,2} nZ_l e \left[\frac{1}{nM_{rl}} \right]^{1/2} \theta_l(z), \quad (3.12)$$

where M_{rl} and $Z_l e$ are the reduced mass and effective charge, respectively, in layer l , and $\theta_l(z) = 1$ in the layer l and $\theta_l(z) = 0$ in the other layer.

Let us assume that the frequencies of all optical modes are about the same and can be replaced by an averaged frequency ω_{av} . Because the energy of an electron is independent of k_z , \mathbf{q}_{\parallel} is determined as $|\mathbf{q}_{\parallel}| = \sqrt{q_x^2 + q_y^2} = q_0^{av}$ to satisfy the energy conservation and q_z is arbitrary ($-\pi/d < q_z < \pi/d$). The summation over j and q_z in Eq. (3.11) can be performed with the use of the closure relation Eq. (2.13),

$$\frac{1}{\tau_{\eta'\eta_{\pm}}(\mathbf{k})} \approx \frac{2\pi e^2}{\hbar} \sum_q \frac{m^*}{q_0^{av} \hbar^2} \delta(q_{\parallel} - q_0^{av}) [n(\omega_{av}) + \frac{1}{2} \pm \frac{1}{2}] \frac{\hbar}{2\omega_{av}} \times \int dr_1^3 \int dr_2^3 \int dr_1'^2 \int_{-d_2}^{d_1} dz_1' \int dr_2'^2 \int_{-d_2}^{d_1} dz_2' \times \sum_{m_1'=0}^{N-1} \sum_{m_2'=0}^{N-1} \psi_{\eta'\mathbf{k}+\mathbf{q}}^*(\mathbf{r}_1) \psi_{\eta\mathbf{k}}(\mathbf{r}_1) \psi_{\eta'\mathbf{k}+\mathbf{q}}(\mathbf{r}_2) \psi_{\eta\mathbf{k}}^*(\mathbf{r}_2) \times \frac{[\mathbf{r}_1 - (\mathbf{r}_1' + m_1' d \mathbf{e}_z)] \cdot [\mathbf{r}_2 - (\mathbf{r}_2' + m_2' d \mathbf{e}_z)]}{\epsilon_{\infty}^2 |\mathbf{r}_1 - (\mathbf{r}_1' + m_1' d \mathbf{e}_z)|^3 |\mathbf{r}_2 - (\mathbf{r}_2' + m_2' d \mathbf{e}_z)|^3} \times \delta(z_1' - z_2') \frac{\exp[iq_z(m_1' - m_2')d]}{N} \times \frac{\exp[i\mathbf{q}_{\parallel} \cdot (\mathbf{r}_{1\parallel}' - \mathbf{r}_{2\parallel}')] }{L^2} \sum_{l=1,2} \frac{nZ_l^2 e^2 \theta_l(z_1')}{M_{rl}}. \quad (3.13)$$

and AlAs-like modes. For $d_1 = d_2 = 113$ Å, the histograms calculated in the envelope-function approximation and the dielectric continuum model are quite similar even for $\Delta\omega = 1$ meV. This shows that the dielectric continuum model is accurate in superlattices with wide layers. For $d_1 = d_2 = 28$ Å, the histograms with $\Delta\omega = 1$ meV differ between the envelope-function approximation and the dielectric continuum model, showing that the latter breaks down for narrow layers, while those with $\Delta\omega = 10$ meV do not. This suggests that the total scattering rate is not sensitive to the details of the model even though differential contributions of individual modes are quite different. We also notice that the sum of the contributions of GaAs-like modes and AlAs-like modes is almost equal to that calculated in the bulk-phonon model.

The reason that the dielectric continuum model and even the bulk-phonon model give reasonable results can be understood by the completeness of phonon modes as follows.⁵¹ In general, we can write the scattering rates as

This shows that the scattering rate does not depend on the details of the displacement of each phonon mode.

This sum rule corresponds to that noted by Mori and Ando¹² in the dielectric continuum model for single heterojunctions and single quantum wells. They expressed the damping rate as

$$\Gamma \cong \frac{\pi}{2} \sum_j \mathcal{A}_j(q_{0j}) \omega_j(q_{0j}) n[\omega_j(q_{0j})] \mathcal{F}_j(q_{0j}), \quad (3.14)$$

where j is the mode index, q_{0j} is the norm of the two-dimensional wave vector for which the energy conservation is satisfied, \mathcal{A}_j is the coupling constant, and \mathcal{F}_j is a form factor. For example, in the case of confined modes in each layer, $\mathcal{A}_j = \alpha_F$ for $\omega_j = \omega_{LO}$ and $\mathcal{A}_j = 0$ for $\omega_j = \omega_{TO}$. They found that the form factors obey a sum rule,

$$\mathcal{F}_B(q_{\parallel}) = \sum_j \mathcal{F}_j(q_{\parallel}), \quad (3.15)$$

where \mathcal{F}_B is the form factor in the bulk-phonon model. It means that as long as $\mathcal{A}_j \omega_j n(\omega_j)$ is nearly independent of j , the damping rate is close to that in the bulk-phonon model. This is the reason why the bulk-phonon model explains the layer-thickness dependence reasonably well. This sum rule is a direct consequence of the closure relation Eq. (2.13).

Note that the validity of the bulk-phonon model is limited to GaAs/AlAs systems at 300 K and that the situation is likely to be quite different in superlattices consisting of other materials. Mori and Ando¹² showed within the dielectric continuum model that the scattering rate can be considerably smaller than that calculated in the bulk-phonon model in AlSb/InAs/AlSb and Ge/InAs/Ge quantum wells.

We have shown in Fig. 7 that $\alpha^2 F$ averaged over GaAs-like modes and over AlAs-like modes in the envelope-function approximation and the dielectric continuum model are in good agreement. This suggests the presence of a completeness relation for GaAs-like modes and AlAs-like modes separately. To prove this, we consider a model in which the displacement is confined to one type of layer with LO-phonon frequency ω_{LO} and the other layer is replaced by an effective medium with a dielectric constant $\epsilon(\omega_{LO})$. In this confined model, the lattice displacement satisfies the completeness in each type of layer. Figure 8 compares the resulting θ dependence of optical modes with a frequency close to that of optical phonons in bulk GaAs with the results in the envelope-function approximation at the Γ point, where $\tan\theta = q_x/q_z$. In Fig. 9, we show the displacement for a GaAs-like mode at $\theta = \pi/4$, where the amount of the dielectric response of the AlAs layer is reinterpreted as the lattice displacement. The calculated polaron damping rate is shown in Fig. 10 together with the result of the envelope-function approximation. All these figures show that the confined model is almost equivalent to the envelope-function approximation.

We can immediately derive an expression of the separate contribution of GaAs- and AlAs-like modes to the relaxation time similar to Eq. (3.13) except that the

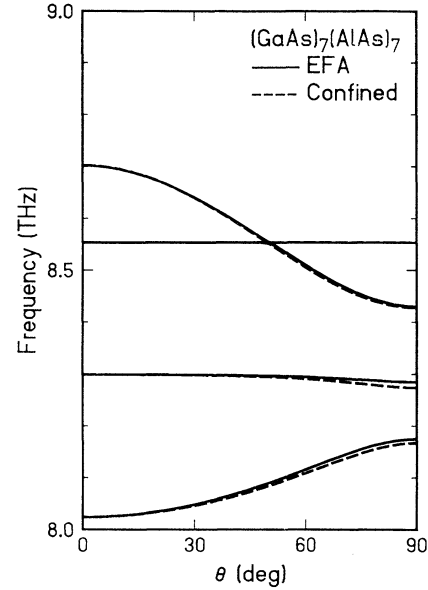


FIG. 8. Dependence of the frequency of modes lying in the vicinity of the LO and TO phonons of GaAs on the wave-vector direction θ ($\tan\theta = q_x/q_z$) at the Γ point. The solid lines represent the results calculated in the envelope-function approximation and the dashed lines those of the confined model.

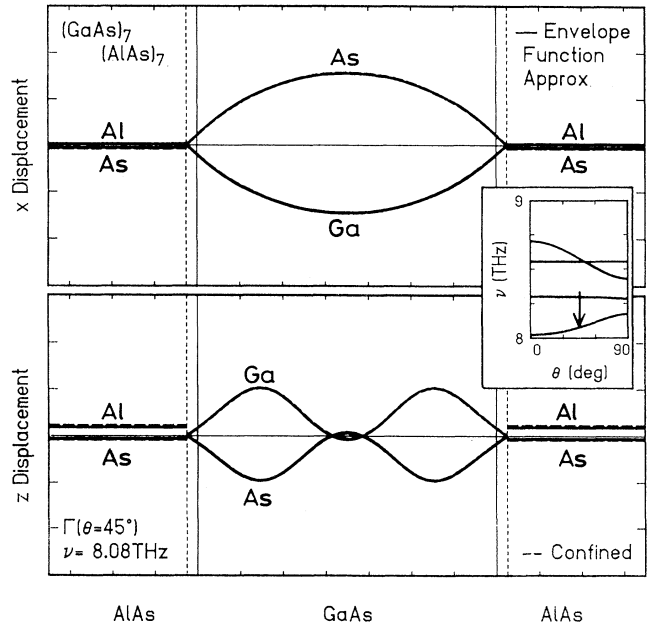


FIG. 9. Calculated displacements of ions for a mode at the Γ point with wave-vector direction $\theta = \pi/4$ and frequency $\nu = 8.08$ THz. The solid lines represent results calculated in the envelope-function approximation and the dashed lines those in the confined model. The thin vertical straight lines indicate the position of the interfacial As planes and the vertical dotted lines the interface position in the envelope-function approximation (Ref. 15).

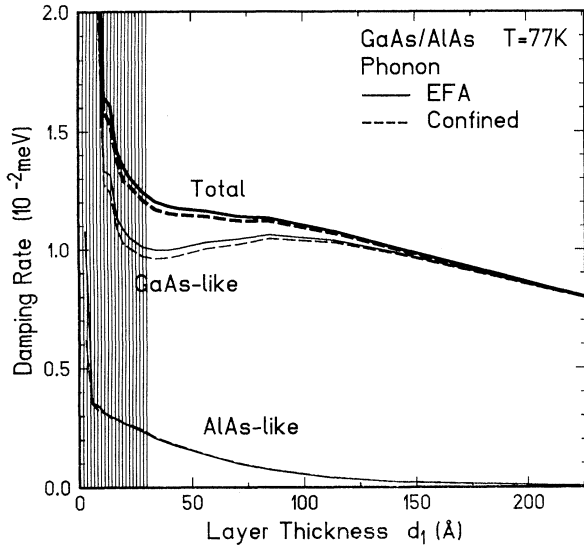


FIG. 10. Layer-thickness d_1 dependence of polaron damping rate calculated in the confined model (dashed lines) and the envelope-function approximation (solid lines) at 77 K. $d_2 = d_1$. The results in the envelope-function approximation are the same as those given in Fig. 2.

sum over l is replaced by a term in which $l=1$ or $l=2$ and that the image effect should be properly included in the relation (2.5) between the potential and the polarization. Therefore, the total contribution of GaAs- or AlAs-like modes is independent of the details of each mode as long as its frequency can be approximated by an average. The same is applicable to the dielectric continuum model, since a similar confined model is equally valid. This explains why the dielectric continuum model successfully gives the electron scattering rates even in superlattices with narrow layers although it cannot describe each phonon mode correctly. It should be noted that the envelope-function approximation is more general than the simpler confined model.

The present calculations show that the electron-optical-phonon interaction becomes stronger as the layer thickness decreases. Opposite results were obtained by some authors. In particular, Riddoch and Ridley⁵² calculated the scattering rate of an electron confined in a thin ionic slab, using the dielectric continuum model, and showed that it decreases as the layer thickness decreases. We can obtain a similar result by neglecting the potential associated with lattice displacements in all layers but the GaAs layer in which an electron is confined.

APPENDIX: ELECTRON-PHONON MATRIX ELEMENTS

A matrix element can be calculated from Eqs. (2.4)–(2.10), (2.12), and (3.3). We have

$$M_{\eta'\eta j\mathbf{q}}(0) = -\frac{2\pi e^2}{\epsilon_\infty} \frac{1}{\sqrt{NL}} \left[\frac{\hbar}{2\omega_j(\mathbf{q})} \right]^{1/2} \times \int_0^{d_1} dz \int_{-d_2}^{d_1} dz'$$

Sawaki⁴² calculated the scattering rate in superlattices, assuming that the optical phonons are completely confined in either layer, and claimed also that the intrasubband scattering rate decreases as the layer width decreases. This is because he completely neglected effects of AlAs-like phonons which become important with decreasing layer thickness.

IV. SUMMARY

In this paper, we have investigated the electron-optical-phonon interactions in GaAs/AlAs superlattices. The envelope-function approximation which reproduces long-wavelength optical phonons quite well was employed. We have found that the results in the dielectric continuum model agree quite well with those in the envelope-function approximation and that even the bulk-phonon model explains the layer-thickness dependence reasonably well.

The Eliashberg function was calculated to determine the extent of contribution of individual modes to the electron scattering. It shows that the dielectric continuum model is quite accurate in superlattices with wide layers but fails to describe individual modes for narrow layers. The total scattering rate, however, turned out to be the same even for narrow layers. This approximate model independence of the total scattering rate was understood in terms of the completeness of the lattice displacement. As a matter of fact, the global completeness of all modes in GaAs and AlAs layers explains why the bulk-phonon model can give a reasonable layer-thickness dependence. A simpler model was introduced in which displacements are totally confined in either GaAs or AlAs layers and other layers are replaced by a continuum which has an appropriate dielectric constant independent of frequency. The approximate validity of this model was established by comparison of frequencies and displacements with those calculated in the envelope-function approximation. The completeness within this confined model explains why the dielectric continuum model gives accurate total scattering rates for both GaAs- and AlAs-like modes even in thin-layer superlattices.

ACKNOWLEDGMENTS

The authors would like to thank Professor Hiroshi Akera for valuable discussions. One of the authors (T.T.) would like to thank Dr. M. Kobayashi, Dr. M. Abe, Dr. T. Mimura, Dr. K. Hikosaka, and Dr. K. Joshin of Fujitsu Laboratories Ltd. for their continuous encouragement. This work is supported in part by the Ministry of Education, Science and Culture, Japan.

$$\begin{aligned} & \times \left\{ \frac{1}{\exp[(q_{\parallel} - iq_z)d] - 1} \psi_{\eta'}^*(z) \psi_{\eta}(z) e^{q_{\parallel}(z-z')} \mathbf{P}_{jq}(z') \cdot (-i\mathbf{e}_{q_{\parallel}} - \mathbf{e}_z) \right. \\ & \quad + \frac{1}{\exp[(q_{\parallel} + iq_z)d] - 1} \psi_{\eta'}^*(z) \psi_{\eta}(z) e^{-q_{\parallel}(z-z')} \mathbf{P}_{jq}(z') \cdot (-i\mathbf{e}_{q_{\parallel}} + \mathbf{e}_z) \\ & \quad \left. + \psi_{\eta'}^*(z) \psi_{\eta}(z) e^{-q_{\parallel}|z-z'|} \mathbf{P}_{jq}(z') \cdot [-i\mathbf{e}_{q_{\parallel}} + \text{sgn}(z-z')\mathbf{e}_z] \right\}, \end{aligned} \quad (\text{A1})$$

where $\mathbf{e}_{q_{\parallel}}$ and \mathbf{e}_z are unit vectors in the direction of \mathbf{q}_{\parallel} and z , respectively. The integration over z and z' can be performed analytically for the electron wave function Eq. (3.4). The result can be expressed as

$$M_{\eta'\eta jq-}(0) = -\frac{2\pi e^2}{\epsilon_{\infty}} \frac{1}{\sqrt{NL}} \left[\frac{\hbar}{2\omega_j(\mathbf{q})} \right]^{1/2} \left\{ \frac{I_E + [-iI_{P-}^x - I_{P-}^z]}{\exp[(q_{\parallel} - iq_z)d] - 1} + \frac{I_E - [-iI_{P+}^x + I_{P+}^z]}{\exp[(q_{\parallel} + iq_z)d] - 1} - iI_{EP}^x + I_{EP}^z \right\}, \quad (\text{A2})$$

where x is chosen in the direction of \mathbf{q}_{\parallel} .

The above expression contains various integrals. First, the integral I_E contains only the information of the electron wave function and is given by

$$\begin{aligned} I_{E\pm} &= \int_0^{d_1} dz \psi_{\eta'}^*(z) \psi_{\eta}(z) e^{\pm q_{\parallel}z} \\ &= \pm \frac{4\eta\eta'\pi^2(q_{\parallel}d_1)[(-1)^{\eta+\eta'}e^{\pm q_{\parallel}d_1} - 1]}{[(q_{\parallel}d_1)^2 + (\eta+\eta')^2\pi^2][(q_{\parallel}d_1)^2 + (\eta-\eta')^2\pi^2]}. \end{aligned} \quad (\text{A3})$$

The integral I_P contains only polarization distribution and is defined as

$$I_{P\pm}^{\alpha} = \int_0^{d_1} dz' P_{jq}^{\alpha}(z') e^{\pm q_{\parallel}z'} = I_{P1\pm}^{\alpha} + I_{P2\pm}^{\alpha} \quad (\text{A4})$$

with $\alpha = x, y$. For phonon modes with amplitude mainly in layer 1, we have

$$I_{P1\pm}^{\alpha} = nZ_1 e \left[\frac{1}{nM_{r1}} \right]^{1/2} \sum_{p=1}^{N_{a1}} C_p^{\alpha} \left[\frac{2}{d_1} \right]^{1/2} d_1 p \pi \frac{1 - (-1)^p e^{\pm q_{\parallel}d_1}}{(q_{\parallel}d_1)^2 + (p\pi)^2} \quad (\text{A5})$$

and

$$I_{P2\pm}^{\alpha} = nZ_2 e \left[\frac{1}{nM_{r2}} \right]^{1/2} e^{\pm q_{\parallel}(d_1+d_2/2)} \left[C_S^{\alpha} \left[\frac{\sinh(q_{\parallel}d_2) + q_{\parallel}d_2}{2q_{\parallel}} \right]^{1/2} \pm C_A^{\alpha} \left[\frac{\sinh(q_{\parallel}d_2) - q_{\parallel}d_2}{2q_{\parallel}} \right]^{1/2} \right], \quad (\text{A6})$$

where C_p^{α} , C_S^{α} , and C_A^{α} are the expansion coefficients defined in Eqs. (2.9) and (2.10). For phonon modes with amplitude mainly in layer 2, on the other hand, we have

$$I_{P1\pm}^{\alpha} = nZ_1 e \left[\frac{1}{nM_{r1}} \right]^{1/2} e^{\pm q_{\parallel}d_1/2} \left[C_S^{\alpha} \left[\frac{\sinh(q_{\parallel}d_1) + q_{\parallel}d_1}{2q_{\parallel}} \right]^{1/2} \pm C_A^{\alpha} \left[\frac{\sinh(q_{\parallel}d_1) - q_{\parallel}d_1}{2q_{\parallel}} \right]^{1/2} \right] \quad (\text{A7})$$

and

$$I_{P2\pm}^{\alpha} = nZ_2 e \left[\frac{1}{nM_{r2}} \right]^{1/2} e^{\pm q_{\parallel}d_1} \sum_{p=1}^{N_{a2}} C_p^{\alpha} \left[\frac{2}{d_2} \right]^{1/2} d_2 p \pi \frac{1 - (-1)^p e^{\pm q_{\parallel}d_2}}{(q_{\parallel}d_2)^2 + (p\pi)^2}. \quad (\text{A8})$$

The integral I_{EP} , which corresponds to the interaction with phonon amplitudes in layer 1, contains both the polarization distribution and electron wave function. For phonon modes with amplitudes mainly in layer 1, we have

$$I_{EP}^x = I_E + I_{P2-}^x + nZ_1 e \left[\frac{1}{nM_{r1}} \right]^{1/2} \sum_{p=1}^{N_{a1}} C_p^x \left[\frac{2}{d_1} \right]^{1/2} d_1 p \pi \frac{\sqrt{2d_1}}{(q_{\parallel}d_1)^2 + (p\pi)^2} \left[I_{E-} - (-1)^p e^{-q_{\parallel}d_1} I_{E+} + \frac{q_{\parallel}d_1}{p\pi} I_{Sp} \right] \quad (\text{A9})$$

and

$$I_{EP}^z = -I_E + I_{P2-}^z + nZ_1 e \left[\frac{1}{nM_{r1}} \right]^{1/2} \sum_{p=1}^{N_{a1}} C_p^z \left[\frac{2}{d_1} \right]^{1/2} d_1 p \pi \frac{\sqrt{2d_1}}{(q_{\parallel}d_1)^2 + (p\pi)^2} \left[I_{E-} + (-1)^p e^{-q_{\parallel}d_1} I_{E+} - I_{Cp} \right], \quad (\text{A10})$$

with

$$I_{Cp} = \begin{cases} -1 & \text{if } \eta + \eta' - p = 0 \\ 1 & \text{if } \eta - \eta' + p = 0 \text{ or } \eta - \eta' - p = 0 \\ 0 & \text{otherwise} \end{cases} \quad (\text{A11})$$

and

$$I_{Sp} = \begin{cases} -\frac{16\eta\eta'p}{\pi[(\eta + \eta')^2 - p^2][(\eta - \eta')^2 - p^2]} & \eta + \eta' + p: \text{ odd} \\ 0 & \text{otherwise} . \end{cases} \quad (\text{A12})$$

For phonon modes with amplitudes mainly in layer 2, on the other hand, we have

$$\begin{aligned} I_{EP}^x = & \frac{4\eta\eta'\pi^2 q_{\parallel} d_1}{[(q_{\parallel} d_1)^2 + (\eta + \eta')^2 \pi^2][(q_{\parallel} d_1)^2 + (\eta - \eta')^2 \pi^2]} \\ & \times \left\{ \frac{1}{2}(C_S^x \beta + C_A^x \gamma) \frac{e^{-q_{\parallel} d_1/2}}{q_{\parallel}} [(-1)^{\eta+\eta'} \cosh(q_{\parallel} d_1) - 1] - (-1)^{\eta+\eta'} d_1 \left[C_S^x \beta \cosh\left(\frac{q_{\parallel} d_1}{2}\right) + C_A^x \gamma \sinh\left(\frac{q_{\parallel} d_1}{2}\right) \right] \right\} \\ & + \left[\frac{(q_{\parallel} d_1)^2 - (\eta + \eta')^2 \pi^2}{[(q_{\parallel} d_1)^2 + (\eta + \eta')^2 \pi^2]^2} - \frac{(q_{\parallel} d_1)^2 - (\eta - \eta')^2 \pi^2}{[(q_{\parallel} d_1)^2 + (\eta - \eta')^2 \pi^2]^2} \right] \left[C_S^x \beta d_1 \sinh\left(\frac{q_{\parallel} d_1}{2}\right) [-(-1)^{\eta+\eta'} - 1] \right. \\ & \left. + C_A^x \gamma d_1 \cosh\left(\frac{q_{\parallel} d_1}{2}\right) [-(-1)^{\eta+\eta'} + 1] \right] \\ & + \left\{ I_{E+} \left[(C_S^x \beta + C_A^x \gamma) d_1 \frac{e^{-q_{\parallel} d_1/2}}{2} - (C_S^x \beta - C_A^x \gamma) d_1 \frac{e^{q_{\parallel} d_1/2}}{2} \frac{e^{-2q_{\parallel} d_1}}{2q_{\parallel}} + I_{P2-} \right] + I_{E-} \frac{e^{q_{\parallel} d_1/2}}{4q_{\parallel}} (C_S^x \beta - C_A^x \gamma) \right\} \end{aligned} \quad (\text{A13})$$

and

$$\begin{aligned} I_{EP}^z = & \frac{4\eta\eta'\pi^2 q_{\parallel} d_1}{[(q_{\parallel} d_1)^2 + (\eta + \eta')^2 \pi^2][(q_{\parallel} d_1)^2 + (\eta - \eta')^2 \pi^2]} \\ & \times \left\{ \frac{1}{2}(C_S^z \beta + C_A^z \gamma) \frac{e^{-q_{\parallel} d_1/2}}{q_{\parallel}} [(-1)^{\eta+\eta'} \cosh(q_{\parallel} d_1) - 1] \right. \\ & \left. + (-1)^{\eta+\eta'} d_1 \left[C_S^z \beta \sinh\left(\frac{q_{\parallel} d_1}{2}\right) + C_A^z \gamma \cosh\left(\frac{q_{\parallel} d_1}{2}\right) \right] \right\} \\ & + \left[\frac{(q_{\parallel} d_1)^2 - (\eta + \eta')^2 \pi^2}{[(q_{\parallel} d_1)^2 + (\eta + \eta')^2 \pi^2]^2} - \frac{(q_{\parallel} d_1)^2 - (\eta - \eta')^2 \pi^2}{[(q_{\parallel} d_1)^2 + (\eta - \eta')^2 \pi^2]^2} \right] \left[C_S^z \beta d_1 \cosh\left(\frac{q_{\parallel} d_1}{2}\right) [(-1)^{\eta+\eta'} - 1] \right. \\ & \left. + C_A^z \gamma d_1 \sinh\left(\frac{q_{\parallel} d_1}{2}\right) [(-1)^{\eta+\eta'} + 1] \right] \\ & - \left\{ I_{E+} \left[(C_S^z \beta + C_A^z \gamma) d_1 \frac{e^{-q_{\parallel} d_1/2}}{2} - (C_S^z \beta - C_A^z \gamma) d_1 \frac{e^{q_{\parallel} d_1/2}}{2} \frac{e^{-2q_{\parallel} d_1}}{2q_{\parallel}} + I_{P2-} \right] + I_{E-} \frac{e^{q_{\parallel} d_1/2}}{4q_{\parallel}} (C_S^z \beta - C_A^z \gamma) \right\} , \end{aligned} \quad (\text{A14})$$

with

$$\beta = \left(\frac{2q_{\parallel}}{\sinh(q_{\parallel} d_1) + q_{\parallel} d_1} \right)^{1/2} \quad (\text{A15})$$

and

$$\gamma = \left(\frac{2q_{\parallel}}{\sinh(q_{\parallel} d_1) - q_{\parallel} d_1} \right)^{1/2} . \quad (\text{A16})$$

- *Present address: Fujitsu Laboratories Ltd., 10-1 Morinosato-Wakamiya, Atsugi 243-01, Japan.
- ¹D. K. Ferry, *Surf. Sci.* **75**, 86 (1978).
 - ²K. Hess, *Appl. Phys. Lett.* **35**, 484 (1979).
 - ³P. J. Price, *Ann. Phys. (N.Y.)* **133**, 217 (1981); *Phys. Rev. B* **30**, 2234 (1984).
 - ⁴F. A. Riddoch and B. K. Ridley, *J. Phys. C* **16**, 6971 (1983).
 - ⁵B. Vinter, *Appl. Phys. Lett.* **45**, 581 (1984).
 - ⁶D. M. Larsen, *Phys. Rev. B* **30**, 4595 (1984).
 - ⁷R. Lassnig, *Phys. Rev. B* **30**, 7132 (1984).
 - ⁸S. Das Sarma and B. A. Mason, *Ann. Phys. (N.Y.)* **163**, 78 (1985).
 - ⁹J. T. Devreese and F. M. Peeters, in *The Physics of the Two-Dimensional Electron Gas*, edited by J. T. Devreese and F. M. Peeters (Plenum, New York, 1987), pp. 131–182, and references cited therein.
 - ¹⁰L. Wendler, R. Haupt, F. Bechstedt, H. Rucker, and R. Enderlein, *Superlatt. Microstruct.* **4**, 577 (1988).
 - ¹¹M. H. Degani and O. Hipólito, *Phys. Rev. B* **35**, 7717 (1987); *Surf. Sci.* **196**, 459 (1988).
 - ¹²N. Mori and T. Ando, *Phys. Rev. B* **40**, 6175 (1989).
 - ¹³H. Rucker, P. Lugli, S. M. Goodnick, and J. E. Lary, *Semicond. Sci. Technol.* **7**, B98 (1992).
 - ¹⁴K. W. Kim, M. A. Littlejohn, M. A. Stroschio, and G. J. Iafrate, *Semicond. Sci. Technol.* **7**, B49 (1992).
 - ¹⁵T. Tsuchiya, H. Akera, and T. Ando, *Phys. Rev. B* **39**, 6025 (1989).
 - ¹⁶T. Tsuchiya and T. Ando, *Semicond. Sci. Technol.* **7**, B73 (1992).
 - ¹⁷M. V. Klein, *IEEE J. Quantum Electron.* **QE-22**, 1760 (1986).
 - ¹⁸B. Jusserand and D. Paquet, in *Semiconductor Heterostructures and Superlattices*, edited by G. Allan *et al.* (Springer, Berlin, 1986), p. 108.
 - ¹⁹B. Jusserand, *Ann. Phys. (Paris)* **13**, 597 (1988).
 - ²⁰D. L. Mills, in *Light Scattering in Solids V*, edited by M. Cardona and G. Güntherodt (Springer, Berlin, 1989), p. 13.
 - ²¹B. Jusserand and M. Cardona, in *Light Scattering in Solids V*, edited by M. Cardona and G. Güntherodt (Springer, Berlin, 1989), p. 49.
 - ²²J. Sapriel and B. Djafari Rouhani, *Surf. Sci. Rep.* **10**, 189 (1989).
 - ²³J. Menéndez, *J. Lumin.* **44**, 285 (1989).
 - ²⁴S. M. Rytov, *Zh. Eksp. Teor. Fiz.* **29**, 605 (1955) [*Sov. Phys. JETP* **2**, 466 (1956)].
 - ²⁵E. P. Pokatilov and S. I. Beril, *Phys. Status Solidi B* **110**, K75 (1982); **118**, 567 (1983).
 - ²⁶R. E. Camley and D. L. Mills, *Phys. Rev. B* **29**, 1695 (1984).
 - ²⁷M. Nakayama, M. Ishida, and N. Sano, *Phys. Rev. B* **38**, 6348 (1988).
 - ²⁸R. Fuchs and K. L. Kliewer, *Phys. Rev.* **140**, A2076 (1965).
 - ²⁹L. Wendler, *Phys. Status Solidi B* **129**, 513 (1985); L. Wendler and R. Haupt, *ibid.* **143**, 487 (1987); **143**, 493 (1987).
 - ³⁰L. Wendler, R. Haupt, and V. G. Grigoryan, *Physica B* **167**, 91 (1990); **167**, 101 (1990); **167**, 113 (1990).
 - ³¹R. Tsu and S. S. Jha, *Appl. Phys. Lett.* **20**, 16 (1972).
 - ³²J. L. Merz, A. S. Barker, Jr., and A. C. Gossard, *Appl. Phys. Lett.* **31**, 117 (1977).
 - ³³A. S. Barker, Jr., J. L. Merz, and A. C. Gossard, *Phys. Rev. B* **17**, 3181 (1978).
 - ³⁴X. X. Liang, S. W. Gu, and D. L. Lin, *Phys. Rev. B* **34**, 2807 (1986); S. W. Gu, X. K. Kong, and G. W. Wei, *ibid.* **36**, 7977 (1987); C. W. Wei, X. J. Kong, and S. W. Gu, *ibid.* **38**, 8390 (1988); S. W. Gu, Y. C. Li, and L. F. Zheng, *ibid.* **39**, 346 (1989).
 - ³⁵N. Sawaki and I. Akasaki, *Physica* **134B**, 494 (1985).
 - ³⁶C. Colvard, T. A. Gant, M. V. Klein, R. Merlin, R. Fischer, H. Morkoç, and A. C. Gossard, *Phys. Rev. B* **31**, 2080 (1985).
 - ³⁷B. Jusserand, D. Paquet, and A. Regreny, *Phys. Rev. B* **30**, 6245 (1984).
 - ³⁸M. Nakayama, K. Kubota, H. Kato, S. Chika, and N. Sano, *Solid State Commun.* **53**, 493 (1985).
 - ³⁹M. Nakayama, K. Kubota, K. Kanata, H. Kato, S. Chika, and N. Sano, *Jpn. J. Appl. Phys.* **24**, 1331 (1985).
 - ⁴⁰E. Molinari, A. Fasolino, and K. Kunc, *Phys. Rev. Lett.* **56**, 1751 (1986).
 - ⁴¹B. Zhu and K. A. Chao, *Phys. Rev. B* **36**, 4906 (1987).
 - ⁴²N. Sawaki, *J. Phys. C* **19**, 4965 (1986).
 - ⁴³B. K. Ridley, *Phys. Rev. B* **39**, 5282 (1989).
 - ⁴⁴M. Babiker, *J. Phys. C* **19**, 683 (1986).
 - ⁴⁵K. Huang and B. F. Zhu, *Phys. Rev. B* **38**, 2183 (1988); **38**, 13377 (1988).
 - ⁴⁶S. Rudin and T. L. Reinecke, *Phys. Rev. B* **41**, 7713 (1990).
 - ⁴⁷H. Rucker, E. Molinari, and P. Lugli, *Phys. Rev. B* **44**, 3463 (1991).
 - ⁴⁸H. Akera and T. Ando, *Phys. Rev. B* **40**, 2914 (1989).
 - ⁴⁹See for example, C. Kittel, *Introduction to Solid State Physics*, 6th ed. (Wiley, New York, 1986), pp. 271–278.
 - ⁵⁰B. K. Ridley and M. Babiker, *Phys. Rev. B* **43**, 9096 (1991).
 - ⁵¹H. Rucker, E. Molinari, and P. Lugli, *Phys. Rev. B* **45**, 6747 (1992). The importance of the completeness of the lattice displacement to the total scattering rate is also discussed in this work.
 - ⁵²F. A. Riddoch and B. K. Ridley, *Physica* **134B**, 342 (1985).